

Stimulated emission reduced fluorescence microscopy: a concept for extending the fundamental depth limit of two-photon fluorescence imaging

Lu Wei, Zhixing Chen, and Wei Min*

Department of Chemistry, Columbia University, New York, NY 10027, USA

*wm2256@columbia.edu

Abstract: Two-photon fluorescence microscopy has become an indispensable tool for imaging scattering biological samples by detecting scattered fluorescence photons generated from a spatially confined excitation volume. However, this optical sectioning capability breaks down eventually when imaging much deeper, as the out-of-focus fluorescence gradually overwhelms the in-focal signal in the scattering samples. The resulting loss of image contrast defines a fundamental imaging-depth limit, which cannot be overcome by increasing excitation efficiency. Herein we propose to extend this depth limit by performing stimulated emission reduced fluorescence (SERF) microscopy in which the two-photon excited fluorescence at the focus is preferentially switched on and off by a modulated and focused laser beam that is capable of inducing stimulated emission of the fluorophores from the excited states. The resulting image, constructed from the reduced fluorescence signal, is found to exhibit a significantly improved signal-to-background contrast owing to its overall higher-order nonlinear dependence on the incident laser intensity. We demonstrate this new concept by both analytical theory and numerical simulations. For brain tissues, SERF is expected to extend the imaging depth limit of two-photon fluorescence microscopy by a factor of more than 1.8.

© 2012 Optical Society of America

OCIS codes: (180.4315) Nonlinear microscopy; (180.2520) Fluorescence microscopy; (190.4180) Multiphoton processes; (170.4090) Modulation techniques.

References and links

1. S. W. Hell, "Far-field optical nanoscopy," *Science* **316**(5828), 1153–1158 (2007).
2. B. Huang, H. Babcock, and X. Zhuang, "Breaking the diffraction barrier: super-resolution imaging of cells," *Cell* **143**(7), 1047–1058 (2010).
3. E. Betzig, G. H. Patterson, R. Sougrat, O. W. Lindwasser, S. Olenych, J. S. Bonifacino, M. W. Davidson, J. Lippincott-Schwartz, and H. F. Hess, "Imaging intracellular fluorescent proteins at nanometer resolution," *Science* **313**(5793), 1642–1645 (2006).
4. W. Denk, J. H. Strickler, and W. W. Webb, "Two-photon laser scanning fluorescence microscopy," *Science* **248**(4951), 73–76 (1990).
5. F. Helmchen and W. Denk, "Deep tissue two-photon microscopy," *Nat. Methods* **2**(12), 932–940 (2005).
6. R. Yuste, ed., *Imaging: a Laboratory Manual* (Cold Spring Harbor Laboratory Press, 2010).
7. P. Theer and W. Denk, "On the fundamental imaging-depth limit in two-photon microscopy," *J. Opt. Soc. Am. A* **23**(12), 3139–3149 (2006).
8. P. Theer, M. T. Hasan, and W. Denk, "Two-photon imaging to a depth of 1000 μm in living brains by use of a Ti:Al₂O₃ regenerative amplifier," *Opt. Lett.* **28**(12), 1022–1024 (2003).
9. D. Kobat, N. G. Horton, and C. Xu, "In vivo two-photon microscopy to 1.6-mm depth in mouse cortex," *J. Biomed. Opt.* **16**(10), 106014 (2011).
10. N. J. Durr, C. T. Weisspennig, B. A. Holfeld, and A. Ben-Yakar, "Maximum imaging depth of two-photon autofluorescence microscopy in epithelial tissues," *J. Biomed. Opt.* **16**(2), 026008 (2011).

11. J. Ying, F. Liu, and R. R. Alfano, "Spatial distribution of two-photon-excited fluorescence in scattering media," *Appl. Opt.* **38**(1), 224–229 (1999).
12. N. Ji, D. E. Milkie, and E. Betzig, "Adaptive optics via pupil segmentation for high-resolution imaging in biological tissues," *Nat. Methods* **7**(2), 141–147 (2010).
13. M. Rueckel, J. A. Mack-Bucher, and W. Denk, "Adaptive wavefront correction in two-photon microscopy using coherence-gated wavefront sensing," *Proc. Natl. Acad. Sci. U.S.A.* **103**(46), 17137–17142 (2006).
14. M. A. A. Neil, R. Juskaitis, and T. Wilson, "Method of obtaining optical sectioning by using structured light in a conventional microscope," *Opt. Lett.* **22**(24), 1905–1907 (1997).
15. Z. Yaqoob, D. Psaltis, M. S. Feld, and C. Yang, "Optical phase conjugation for turbidity suppression in biological samples," *Nat. Photonics* **2**(2), 110–115 (2008).
16. A. Leray, K. Lillis, and J. Mertz, "Enhanced background rejection in thick tissue with differential-aberration two-photon microscopy," *Biophys. J.* **94**(4), 1449–1458 (2008).
17. N. Chen, C. H. Wong, and C. J. Sheppard, "Focal modulation microscopy," *Opt. Express* **16**(23), 18764–18769 (2008).
18. W. Min, S. Lu, S. Chong, R. Roy, G. R. Holtom, and X. S. Xie, "Imaging chromophores with undetectable fluorescence by stimulated emission microscopy," *Nature* **461**(7267), 1105–1109 (2009).
19. W. Min, "Label-free optical imaging of nonfluorescent molecules by stimulated radiation," *Curr. Opin. Chem. Biol.* **15**(6), 831–837 (2011).
20. J. B. Ding, K. T. Takasaki, and B. L. Sabatini, "Supraresolution imaging in brain slices using stimulated-emission depletion two-photon laser scanning microscopy," *Neuron* **63**(4), 429–437 (2009).
21. P. Bianchini, B. Harke, S. Galiani, G. Vicidomini, and A. Diaspro, "Single-wavelength two-photon excitation-stimulated emission depletion (SW2PE-STED) superresolution imaging," *Proc. Natl. Acad. Sci. U.S.A.* **109**(17), 6390–6393 (2012).
22. S. W. Hell, "Microscopy and its focal switch," *Nat. Methods* **6**(1), 24–32 (2009).
23. K. Isobe, A. Suda, H. Hashimoto, F. Kannari, H. Kawano, H. Mizuno, A. Miyawaki, and K. Midorikawa, "High-resolution fluorescence microscopy based on a cyclic sequential multiphoton process," *Biomed. Opt. Express* **1**(3), 791–797 (2010).

1. Introduction

Advances in optical imaging techniques have revolutionized our ability to study biological structures and functions on microscopic scales. For a given optical imaging modality, the spatial resolution and the penetration depth are two crucial technical parameters. While the diffraction limited spatial resolution has been broken by a few seminal techniques such as STED microscopy [1–3], the best penetration depth for living organisms is exhibited by two-photon (2P) microscopy, which can provide high-resolution (sub-cellular) images deep within scattering samples [4]. Due to the nonlinear intensity dependence of the absorption, 2P excited fluorescence is mostly generated from the laser focus. Such a spatially confined excitation allows efficient capture of the emitted and subsequently scattered fluorescence by a large-area detector without a confocal pinhole, which dramatically promotes the detection sensitivity deep within scattering samples [5]. As such, 2P microscopy is now an indispensable tool in the arsenal of biophotonics [6].

However, 2P microscopy is still constrained by a fundamental imaging-depth limit for scattering samples. This depth limit for most cases is not limited by the available laser power but rather by the obtainable image contrast [7–11]. As shown in Fig. 1(a), the 2P image of fluorescent beads embedded in a turbid 3D sample gradually fades away with depth. The corresponding depth limit is, however, not the true maximum. When the laser power is increased accordingly, images can be acquired much deeper. Nevertheless, the image contrast deteriorates with depth as shown in Fig. 1(b). Eventually, it is no longer feasible to identify the target beads from the overwhelming background, regardless of how much laser power is applied. For mouse brain tissues expressing GFP, the corresponding depth limit is about 1 mm [8]. Although this depth is impressive compared with other high-resolution techniques, it still covers only a very small fraction of the mammalian brain.

Such a fundamental imaging-depth limit arises because, as the required incident laser power increases with imaging depth in order to maintain the same excitation power at focus, the conventional wisdom that 2P fluorescence is generated only within the focal volume no longer holds [7]. Eventually, the fluorescence from out-of-focus fluorophores (especially those located near the sample surface) will grow and dominate the detected signal (Fig. 1(c)).

The fundamental imaging-depth limit can be defined as

$$\left(\frac{S}{B}\right)_{2P} = \frac{\int_{V_{in}} \int_0^\tau C_S(r, z) I^2(r, z, t) dt dV}{\int_{V_{out}} \int_0^\tau C_B(r, z) I^2(r, z, t) dt dV} = 1 \quad (1)$$

where V_{in} is the focal volume, V_{out} is the total sample volume along the beam path but excluding the focal volume, r is the distance from the optical axis, z is the axial distance from the tissue surface, C is the local fluorophore concentration, I is the laser intensity, and τ is the pixel dwell time during the imaging. We assume equal fluorescence collection efficiency between signal and background at the large-area detector. As an analogy, the limited imaging-depth here is reminiscent to the scenario of wide-field fluorescence microscopy which lacks background rejection.

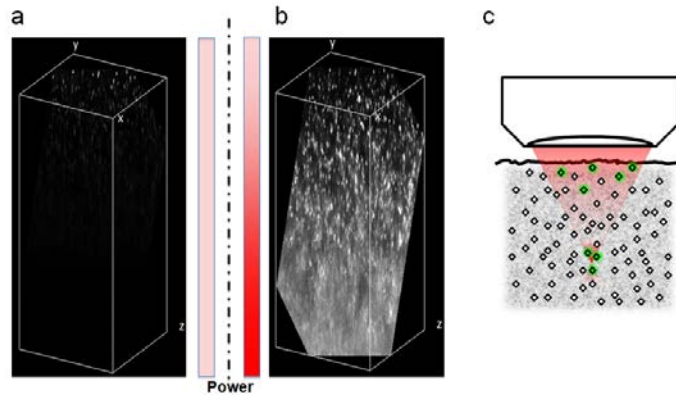


Fig. 1. Demonstration of the fundamental imaging-depth limit of two-photon microscopy. (a) Under constant two-photon excitation power, volume images of a turbid gel sample doped with fluorescent beads exhibit a decreasing fluorescence signal over depth. (b) Deeper images can be acquired for the same sample when using compensating higher laser power in deeper layers. However, increasingly reduced signal-to-background ratio was observed. (c) The reduced image contrast when imaging deep inside the sample is due to the inevitable excitation of out-of-focus fluorophores. A formal definition of fundamental imaging-depth limit of two-photon microscopy is where fluorescence signal generated from in-focus and from out-of-focus are comparable.

Obviously, this fundamental depth limit cannot be overcome by further increasing the laser power, which would unbiasedly enhance both signal and background. Since the loss of intensity due to sample scattering is the physical origin of the imaging-depth limit, one should be able to design and tailor incident waves that could experience less scattering within a given turbid sample. Indeed, extensive efforts have been made along this wave-based strategy, such as adaptive optics [12,13], imaging with structured illumination [14], longer excitation wavelengths [9], optical phase conjugation [15], differential aberration imaging [16] and focal modulation [17].

Herein we propose a novel spectroscopy-based concept, Stimulated Emission Reduced Fluorescence (SERF) Microscopy, to extend the fundamental depth limit of 2P fluorescence imaging. Stimulated emission (S.E.) has been the key switching mechanism in STED microscopy for breaking the diffraction-limited spatial resolution [1], and recently was employed as a new contrast mechanism for imaging non-fluorescent chromophores with superb sensitivity [18,19]. In SERF, we adopt a scheme that combines a continuous wave (CW) S.E. beam collinearly with 2P beam and detects the reduced fluorescence signal. By choosing a S.E. beam with proper wavelength and intensity to preferentially switch off the fluorescence signal from the focus while keeping most of the out-of-focus background

fluorescence less affected, SERF will promote the image contrast of in-focus signal over out-of-focus background, effectively extending the fundamental imaging depth limit. Both analytical and numerical results will be presented to support our proposal.

2. Theory

2.1. Laser intensity distribution inside scattering samples

We first analyze how the laser intensity is distributed within the scattering sample when the depth limit is reached for regular 2P imaging. Fluorophores are normally distributed throughout the 3D volume of the sample. Thus, the number of out-of-focus fluorophores is almost always orders-of-magnitude larger than that of the in-focus ones:

$$\frac{\int_{V_{in}} C_S(r, z) dV}{\int_{V_{out}} C_B(r, z) dV} \ll 1 \quad (2)$$

The comparison between Eq. (1) and Eq. (2) indicates that, despite of the scattering loss, $I^2(r, z)$ at the focus will be much larger than its out-of-focus counterpart when the depth limit is reached as defined in Eq. (1). In a simplified condition with a homogeneous fluorophore distribution, i.e., $C_B(r, z) = C_S(r, z)$, $\int_V \int_0^t I^2(r, z, t) dt dV$ will be equal between the background and the signal. Consequently, the integral of $I^2(r, z)$ over a subset of the out-of-focus volume will also be smaller than that over the focus.

2.2. Reduced fluorescence in the presence of stimulated emission

Additionally, we quantify the reduced fluorescence effect when combining a CW S.E. beam collinearly with a 2P excitation beam and focusing them into a common focal spot.

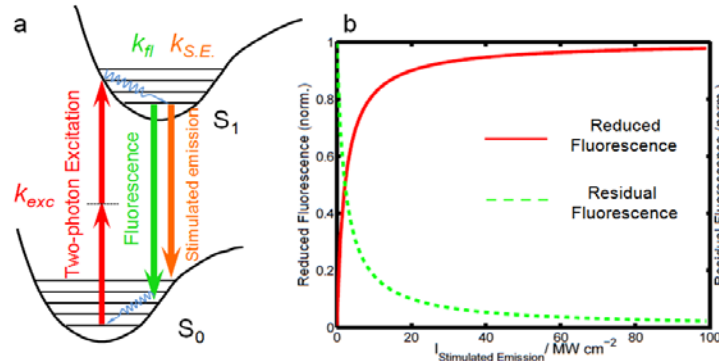
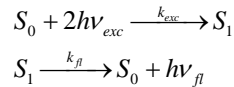


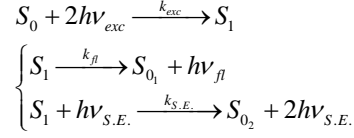
Fig. 2. (a) A simplified Jablonski diagram of a typical fluorophore under two-photon excitation and one-photon stimulated emission. (b) The intensity dependence of reduced fluorescence and residual fluorescence on the S.E. beam. $\tau_f = 10$ ns, $\lambda_{S.E.} = 750$ nm, $\sigma_{S.E.} = 10^{-17}$ cm².

Assuming no fluorescence saturation or photobleaching, below we analyze the following two photophysical schemes of 2P fluorescence with and without the S.E. beam.

In the absence of the S.E. beam,



In the presence of the S.E. beam,



where S_0 and S_1 represent the ground and the excited state, respectively, $h\nu$ is the energy of a single photon, $k_{exc} = \sigma_{exc}(I_{exc}\lambda_{exc}/hc)^2$ is the 2P excitation rate, σ_{exc} is the 2P absorption cross-section of the molecule at λ_{exc} , and I_{exc} is the intensity of the 2P excitation beam (in W/cm²). The fluorescence emission rate k_{fl} is a constant for a given fluorophore: $k_{fl} = 1/\tau_{fl}$, where τ_{fl} is the fluorescence lifetime. In the case of S.E., $k_{S.E.} = \sigma_{S.E.} I_{S.E.} \lambda_{S.E.}/hc$ is the S.E. rate, where $\sigma_{S.E.}$ is the S.E. cross-section of the molecule at $\lambda_{S.E.}$. Thus we can calculate the 2P fluorescence emission rate of a single fluorescent molecule (R) and its counterpart in the presence of S.E. attenuation (R'):

$$R = f_{rep} k_{exc} \tau_{exc} \eta \quad (3a)$$

$$R' = f_{rep} k_{exc} \tau_{exc} \eta' = f_{rep} k_{exc} \tau_{exc} \eta \frac{k_{fl}}{k_{fl} + k_{S.E.}} \quad (3b)$$

where f_{rep} is repetition rate of the excitation pulse train, τ_{exc} is the pulse width (~ 100 fs for a typical 2P laser), η is the fluorescence quantum yield, and η' is effective fluorescence quantum yield in the presence of the S.E. beam. Subtracting Eq. (3b) from Eq. (3a), we obtain the reduced fluorescence rate (defined as R_{SERF}) as

$$R_{SERF} \equiv R - R' = f_{rep} k_{exc} \tau_{exc} \eta \frac{k_{S.E.}}{k_{fl} + k_{S.E.}} \quad (4)$$

Different from the commonly known STED signal, in which the residual fluorescence decreases with the increasing S.E. beam intensity, R_{SERF} increases with the intensity of S.E. beam (Fig. 2(b)) due to its differential nature.

2.3. Imaging contrast of SERF

Taking R_{SERF} in Eq. (4) back into Eq. (1), we get the image contrast $(S/B)_{SERF}$ of SERF in the differential imaging mode,

$$\left(\frac{S}{B}\right)_{SERF} = \frac{\int_{V_{in}} \int_0^\tau C_S(r, z) \frac{\alpha I_{S.E.}(r, z)}{1 + \alpha I_{S.E.}(r, z)} I_{exc}^2(r, z, t) dt dV}{\int_{V_{out}} \int_0^\tau C_B(r, z) \frac{\alpha I_{S.E.}(r, z)}{1 + \alpha I_{S.E.}(r, z)} I_{exc}^2(r, z, t) dt dV} \quad (5)$$

where $\alpha \equiv \tau_{fl} \sigma_{S.E.} \lambda_{S.E.}/hc$. For many red fluorophores, $\lambda_{S.E.}$ and λ_{exc} can be chosen to be close or even identical to each other. Consequently, 2P and S.E. beams would both lie within the tissue transparency window (650–1300 nm) and experience similar attenuation effects inside scattering samples. As analyzed earlier, $I_{exc}(r, z, t)$ at the focus is much more intense than its out-of-focus counterpart when reaching the depth limit of regular 2P imaging. Consequently, $I_{S.E.}(r, z)$ and $\alpha I_{S.E.}(r, z)/[1 + \alpha I_{S.E.}(r, z)]$ at the focus should be much higher than their out-of-focus counterparts as well. Therefore, by introducing a new factor of $\alpha I_{S.E.}(r, z)/[1 + \alpha I_{S.E.}(r, z)]$, which makes the intensity ratio between the in focus and out of

focus part even larger, we can preferentially switch off the molecules in the focus but not in the background, and claim an improved signal-to-background contrast at the original 2P imaging depth limit with SERF (i.e., $(S/B)_{SERF} > (S/B)_{2P} = 1$).

A cartoon in Fig. 3 visually presents the principle of SERF. By subtracting the residual 2P fluorescence signal (in the presence of S.E. beam) from the original 2P fluorescence signal (without the S.E. beam) at each point, reduced fluorescence signal is preferentially generated at focal point, which will enhance the image contrast.

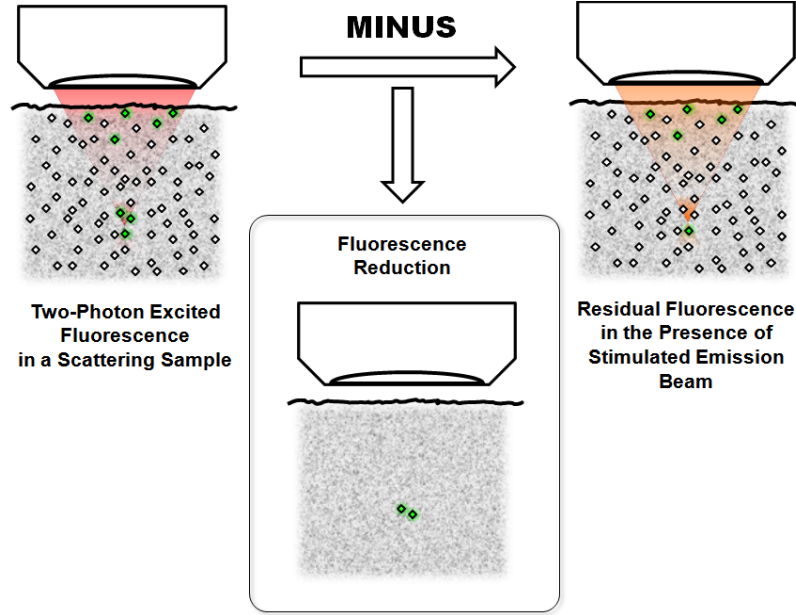


Fig. 3. Cartoon representation of the principle of SERF. Stimulated emission beam preferentially reduces the in-focus fluorescence signal over out-of-focus background fluorescence due to its intensity distribution disparity. The resulting differential signal would be mainly generated from the laser focus. Consequently, images reconstructed with the differential signal are expected to exhibit a higher contrast when comparing with original two-photon fluorescence image.

2.4. Imaging contrast dependence of S.E. intensity $I_{S.E.}$

We now address how the image contrast of SERF depends on the applied S.E. beam intensity $I_{S.E.}$. When $I_{S.E.}$ is very large, it will lead to $\alpha I_{S.E.}(r, z)/[1 + \alpha I_{S.E.}(r, z)] \sim 1$ in Eq. (5), which results in $(S/B)_{SERF} \sim (S/B)_{2P} = 1$. This is so because the switching-off effect becomes unbiased for fluorophores in the focus and at background with no further contrast improvement being achieved. On the other hand, when the reduced fluorescence is in the linear (non-saturating) condition, more specifically, when $\alpha I_{S.E.}(r, z) < 1$ and the reduced fluorescence is beyond the shot noise, $(S/B)_{SERF}$ becomes

$$\left(\frac{S}{B}\right)_{SERF} \approx \frac{\int_{V_{in}} \int_0^{\tau} C_S(r, z) I_{S.E.}(r, z) I_{exc}^2(r, z, t) dt dV}{\int_{V_{out}} \int_0^{\tau} C_B(r, z) I_{S.E.}(r, z) I_{exc}^2(r, z, t) dt dV} > 1 \quad (6)$$

Equation (6) directly reveals the physical picture underlying the SERF method: when operating above the shot noise of both the signal and the background with long enough signal acquisition time, SERF transforms the originally 2P nonlinear process into an overall three-

photon process by adding a S.E. laser beam instead of another virtual state. The ascending of this high-order nonlinearity improves the S/B ratio, thereby improving the contrast and extending the imaging depth into scattering samples.

3. Experimental designs

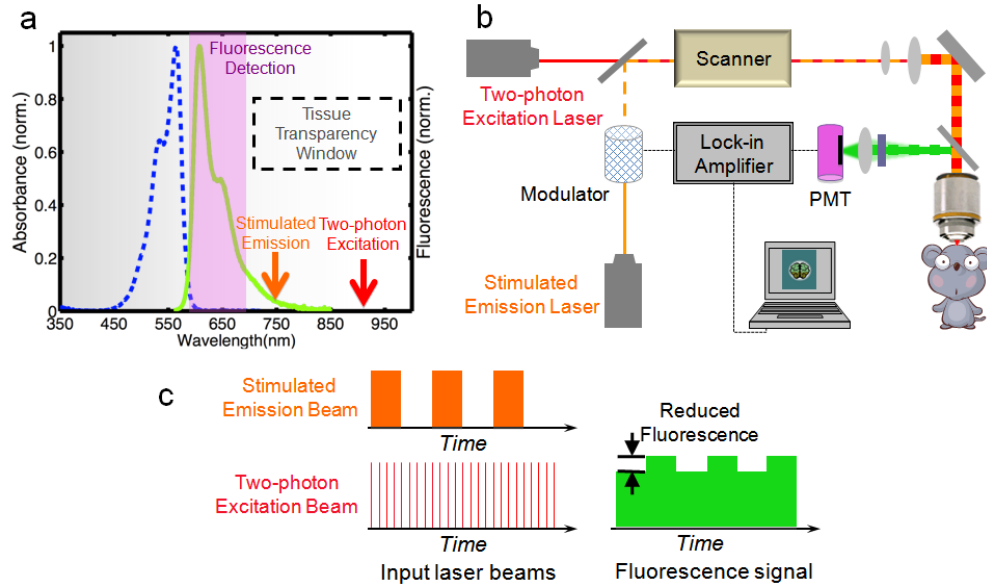


Fig. 4. Proposed experimental design of SERF. (a) Absorption and fluorescence spectrum of a red emission dye candidate for SERF. Both the stimulated emission and the 2-photon excitation wavelength are in the tissue transparency window for *in vivo* imaging. (b) SERF setup. In addition to a standard two-photon fluorescence microscope, a modulated stimulated emission beam is combined collinearly with the two-photon excitation beam. Reduced fluorescence at each pixel is measured by a lock-in amplifier. (c) Modulation transfer scheme of SERF. The stimulated emission beam is modulated at a high frequency ($> \text{MHz}$), which accounts for the reduced fluorescence modulated at the same frequency after interacting with fluorophores.

3.1. SERF fluorophores

Generally speaking, all fluorophores studied with STED microscopy can be used in SERF. Fluorophores having high 2P absorption cross-section, high brightness, broad and red-shifted emission spectra with a reasonably large Stokes shift are particularly suitable. Figure 4(a) shows the absorption and emission spectra for an applicable red-emitting fluorophore, overlaid with the 2P excitation wavelength, S.E. wavelength and the spectral window for fluorescence collection. It has been already shown [20] that fluorophores excited via 2P processes can be forced back to the ground state via one-photon STED in the near IR region, which supports our SERF design. It is worth stressing that the chosen wavelengths of S.E. beam and 2P excitation beam would be close to each other and both within tissue transparency window, making them behave similarly in terms of the scattering effect.

3.2. SERF microscope setup

Figure 4(b) shows the proposed SERF experiment setup. A 2P fluorescence microscope is equipped with a widely tunable pulsed laser and a non-descanned photomultiplier tube (PMT) detector closely attached to the objective to maximize the collection efficiency. Collinearly combined with the 2P laser beam, a CW S.E. laser beam is intensity modulated by a modulator at a high frequency ($\sim 5 \text{ MHz}$). The reduced fluorescence signal induced at the modulation frequency will be picked out by a lock-in amplifier connected after the PMT. The implementation of high frequency modulation and demodulation technique will be helpful for

removing slow laser intensity noise as in other modulation transfer techniques [19]. Hence, we only need to consider the shot noise for SERF. The designed pulse train of 2P beam, CW S.E. beam and the resulting reduced fluorescence signal are illustrated in Fig. 4(c). According to Fig. 2(b), we design that the S.E. beam intensity is about 5–10 MW/cm² at focus to reduce the in-focus fluorescence by ~50% (which is just across the linear range), so that the reduced fluorescence signal won't be saturated through the sample volume to sacrifice the S/B .

4. Numerical simulation

Equation (6) has proven that, in a non-saturating condition of S.E., SERF can attain $(S/B)_{SERF} > (S/B)_{2P} = 1$ by imaging the reduced fluorescence at the imaging-depth limit of the regular 2P microscopy defined in Eq. (1). Here we evaluate the advantage of SERF in deep tissue imaging by numerical simulation using *Matlab*.

4.1. Available laser power inside scattering sample

For a propagating Gaussian beam, the z -dependent beam area, $A(z)$, follows:

$$A(z) \propto 1 + \left[\frac{(z - z_{focal})}{z_R} \right]^2 \quad (7)$$

where $z_R = \pi\omega_0^2 / \lambda$ is the Rayleigh range, ω_0 is the beam waist, and z_{focal} denotes the focal depth below the sample surface ($z = 0$). We adopt $z_R = 0.5 \mu\text{m}$ for a typical microscope objective. When focusing the 2P beam and S.E. beam deep into the scattering sample, the ballistic part of the Gaussian beam follows a Lambert-Beer-like exponential decline with imaging depth [5]. For the sake of performing analytical treatment, only the ballistic light is considered for samples whose anisotropy factors are low or moderate [7]. The area-integrated light power at certain z depth below surface thus can be described as

$$P_{ballistic}(z) = P_0 e^{-z/L_s} \quad (8)$$

where P_0 is the light power at sample surface, and L_s is the mean free path length describing the scattering strength. For example, $L_s \approx 200 \mu\text{m}$ for brain tissues in the near IR region [5].

4.2. The imaging depth limit of regular two-photon microscopy

Assuming uniformly fluorophore-stained sample and uniformly distributed laser intensity for each z layer, we can integrate dt , dr first in Eq. (1) for the regular 2P imaging case:

$$\left(\frac{S}{B} \right)_{2P} \approx \frac{\int_{z_{in}}^{z_{out}} \int_0^{r(z)} I_{ballistic}^2(r, z) dr dz}{\int_{z_{out}}^{z_{in}} \int_0^{r(z)} I_{ballistic}^2(r, z) dr dz} \approx \frac{\int_{z_{in}}^{z_{out}} \left[\frac{P_{ballistic}(z)}{A(z)} \right]^2 A(z) dz}{\int_{z_{out}}^{z_{in}} \left[\frac{P_{ballistic}(z)}{A(z)} \right]^2 A(z) dz} \quad (9)$$

By defining $Q(z)_{2P} \equiv [P_{ballistic}(z)/A(z)]^2 A(z)$ and plugging in $A(z)$ and $P_{ballistic}(z)$ in Eqs. (7) and (8), we have

$$Q(z)_{2P} \propto \frac{\exp(-2z/L_s)}{1 + \left[\frac{(z - z_{focal})}{z_R} \right]^2} \quad (10)$$

To find out the corresponding z_{focal} limit that achieves $S/B = 1$, we use the function “quadgk” in Matlab adopting Gauss–Kronrod quadrature formula, which has a relative error tolerance as $1.0e^{-6}$, to numerically integrate both the fluorescence signal around focus and out of the focus as follows:

$$\left(\frac{S}{B}\right)_{2P} \approx \frac{\int_{z_{focal}-\varepsilon}^{z_{focal}+\varepsilon} Q(z)_{2P} dz}{\int_0^{z_{focal}-\varepsilon} Q(z)_{2P} dz} = 1 \quad (11)$$

As shown in Fig. 5(a), by reasonably assigning $\varepsilon = 1 \mu\text{m}$, which is about two times the full width at half-maximum (FWHM) of the signal peak and whose actual value is not very sensitive, the numerical integration shows that the imaging-depth limit for regular 2P imaging is reached when $z_{focal} = 1023 \mu\text{m}$. This result is in fact very close to the experimentally measured value of 1 mm for brain tissues [8].

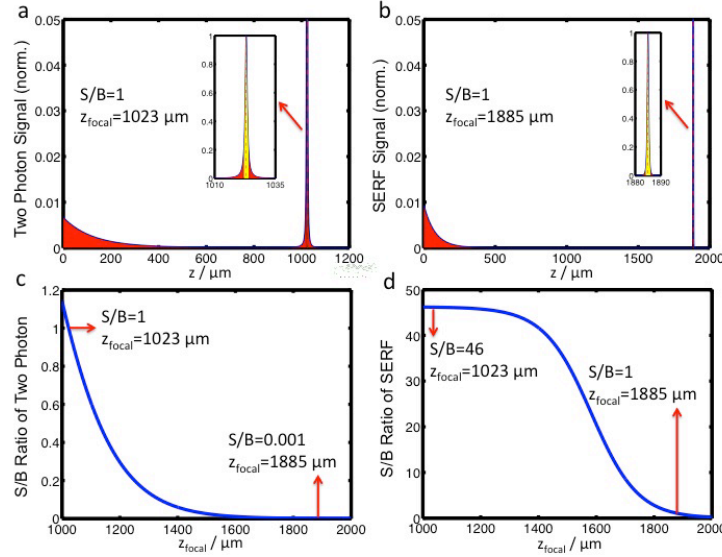


Fig. 5. Comparison of the fundamental imaging-depth limit between the regular two-photon imaging and SERF. (a) Using the typical parameters described in the text, the fundamental depth limit for two-photon imaging is $1023 \mu\text{m}$ at which $(S/B)_{2P} = 1$. The yellow part beneath the curve is the integrated in-focus signal with a width of $2 \mu\text{m}$, the red part with the z less than focus is the integrated out-of-focus background. Signal curve shown here has been normalized to the peak value of the signal. (b) The new depth limit for SERF is determined in a similar way, and is found to be $1885 \mu\text{m}$ when $(S/B)_{SERF} = 1$, extending the depth by more than 1.8 times. (c) The dependence of $(S/B)_{2P}$ as a function of the focal depth z_{focal} between $1000 \mu\text{m}$ and $2000 \mu\text{m}$. At the SERF extended depth limit of $1885 \mu\text{m}$, $(S/B)_{2P}$ is only 0.001. (d) On the contrary, when at the regular 2P depth limit of $1023 \mu\text{m}$, $(S/B)_{SERF}$ is 46, which is much higher than the corresponding $(S/B)_{2P} = 1$ at this focal depth.

4.3. S/B improvement and depth extension of SERF

It has been shown in Eq. (6) that SERF method is an overall three-photon nonlinear process. Again, by assuming uniformly stained sample and uniformly distributed laser intensity in each z layer, we can modify Eq. (6) into

$$\left(\frac{S}{B}\right)_{SERF} \approx \frac{\int_{z_{in}}^{z_{out}} \int_0^{r(z)} I_{ballistic}^3(r, z) dr dz}{\int_{z_{out}}^{z_{in}} \int_0^{r(z)} I_{ballistic}^3(r, z) dr dz} \approx \frac{\int_{z_{in}}^{z_{out}} \left[\left(\frac{P_{ballistic}(z)}{A(z)}\right)^3 A(z)\right] dz}{\int_{z_{out}}^{z_{in}} \left[\left(\frac{P_{ballistic}(z)}{A(z)}\right)^3 A(z)\right] dz} \quad (12)$$

By defining $Q(z)_{SERF} \equiv \left[\frac{P_{ballistic}(z)}{A(z)}\right]^3 A(z)$, we have

$$Q(z)_{SERF} \propto \frac{\exp(-3z/L_s)}{\left(1 + \left[(z - z_{focal})/z_R\right]^2\right)^2} \quad (13)$$

Similar numerical integration can be done for SERF as in the 2P imaging described in Eq. (11). Figure 5(b) shows that, by using SERF, $(S/B)_{SERF} = 1$ is reached at a new depth limit of $z_{focal} = 1885 \mu\text{m}$. This effectively extends the original depth limit of $z_{focal} = 1023 \mu\text{m}$ of regular 2P imaging by more than 1.8 times. A more systematic study in Figs. 5(c) and 5(d) shows how the image contrast diminishes with the increasing imaging depth for both regular 2P imaging and SERF. SERF can achieve a 46 times of S/B contrast improvement when imaging at regular 2P depth limit of $z_{focal} = 1023 \mu\text{m}$. Note that we assume a long enough integration time here so that the shot noise can be neglected. As a reference, regular 2P imaging can only exhibit $S/B = 0.001$ at the corresponding SERF depth limit of $z_{focal} = 1885 \mu\text{m}$. Even though here we only analyze samples with low or moderate anisotropy factors, similar qualitative conclusion is expected for samples with near-unity anisotropy factor.

5. Discussion

It is imaginable to extend the depth limit of 2P microscopy by detecting three-photon (or four-photon) excited fluorescence signal. However, this seemingly viable approach is not practically attractive for bio-imaging, because (1) the simultaneous three-photon (or four-photon) absorption via more virtual states is an extremely improbable event: the transition amplitude is determined by the fifth (or seventh) order nonlinear molecular polarizability, and (2) the laser excitation wavelength for the classic GFP, YFP and RFP needs to be longer than 1400 nm, which lies outside the tissue transparency window (650–1300 nm) of most biological tissues. In contrast, SERF works through the real excited state of the fluorophore and all the involved wavelengths are within the tissue transparency window.

Although the current SERF setup employs a separate CW laser beam for S.E., one might be able to perform single wavelength experiment with the proper fluorophores (single-wavelength STED has been recently demonstrated on ATTO647N [21]). In this case, the 2P excitation wavelength lies within the fluorescence emission spectrum of the fluorophores. Experimentally, the output of a femtosecond pulsed laser is spitted into two arms, and one of the pulse trains is stretched into long pulses to act as the CW beam for S.E.

Finally, it is highly constructive to compare the technical aspects of SERF with STED microscopy [22], as both techniques are harnessing the fluorescence quenching process under S.E. First, STED aims to break the spatial resolution limit while SERF is designed to extend the penetration depth. Second, the S.E. beam in STED is spatially shaped while the S.E. beam in SERF is being temporally modulated. Third, STED measures the residual fluorescence signal in the focus while SERF measures the difference between the original and residual fluorescence signals. Finally, STED works best in the fluorescence depletion region while SERF has to work in the non-saturating region in order to perform deep imaging. It is worth pointing out that, while SERF can improve the imaging depth, it should also be able to enhance the spatial resolution as implied in a recent report using high-order nonlinearity [23].

6. Conclusion

In summary, a new fluorescence microscopy, SERF, is proposed to extend the fundamental depth limit of 2P imaging. This concept is radically different from the existing strategies that focus on ways to reduce scattering loss of the incident light. Technically, SERF is rather straightforward, as only a near IR CW laser beam (and the associated modulation electronics) is needed to be incorporated onto a standard 2P fluorescence microscope. We demonstrated, both analytically and numerically, the advantage of SERF method in terms of acquiring high-contrast images deep inside scattering samples. In particular, a 1.8-times deeper imaging depth is expected for scattering samples such as brain tissues.

Acknowledgments

We thank Ya-Ting Kao, Xinxin Zhu, Louis Brus, Rafael Yuste, Darcy Peterka, Virginia Cornish, Christophe Dupre and Miguel Jimenez for helpful discussions. W. M. acknowledges the startup funds from Columbia University, and grant support from Kavli Institute for Brain Science.